"Modeling Diffusive Search by Non-Adaptive Sperm: Empirical and Computational Insights"

Short title: 'Modeling Sperm Diffusive Search'

Benjamin M. Brisard[1*], Kylie D. Cashwell[1*], Stephanie M. Stewart[1], Logan M. Harrison[1], Aidan C. Charles[1], Chelsea V. Dennis[1], Ivie R. Henslee[1], Ethan L. Carrow[1], Heather A. Belcher[2], Debajit Bhowmick[3], Paul W. Vos[4], Maciej Majka[5], Martin Bier[6], David M. Hart[7], Cameron A. Schmidt[1**]

[1]Department of Biology, East Carolina University, Greenville NC

[2]Department of Anatomy and Cell Biology, Brody School of Medicine, East Carolina University

[3]Flow Cytometry Core Facility, Brody School of Medicine, East Carolina University

[4]Department of Public Health, East Carolina University, Greenville NC

[5] Institute of Theoretical Physics and Mark Kac Center for Complex Systems Research, Jagiellonian University, Krakow, Poland

[6]Department of Physics, East Carolina University, Greenville NC

[7]Department of Computer Science, East Carolina University, Greenville, NC

*These authors contributed equally to the work.

**Corresponding author: Cameron A. Schmidt (schmidtc18@ecu.edu)

Abstract

During fertilization, mammalian sperm undergo a winnowing selection process that reduces the candidate pool of potential fertilizers from ~10^6-10^{11} cells to 10^1-10^2 cells (depending on the species). Classical sperm competition theory addresses the positive or 'stabilizing' selection acting on sperm phenotypes within populations of organisms but does not strictly address the developmental consequences of sperm traits among individual organisms that are under purifying selection during fertilization. It is the latter that is of utmost concern for improving assisted reproductive technologies (ART) because 'low fitness' sperm may be inadvertently used for fertilization during interventions that rely heavily on artificial sperm selection, such as intracytoplasmic sperm injection (ICSI). Importantly, some form of sperm selection is used in nearly all forms of ART (e.g., differential centrifugation, swim-up, or hyaluronan binding assays, etc.). To date, there is no unifying quantitative framework (i.e., theory of sperm selection) that synthesizes causal mechanisms of selection with observed natural variation in individual sperm traits. In this report, we reframe the physiological function of sperm as a collective diffusive search process and develop multi-scale computational models to explore the causal dynamics that constrain sperm 'fitness' during fertilization. Several experimentally useful concepts are developed, including a probabilistic measure of sperm 'fitness' as well as an information theoretic measure of the magnitude of sperm selection, each of which are assessed under systematic increases in microenvironmental selective pressure acting on sperm motility patterns.

Author Summary

Fertilization in mammals requires many orders of magnitude more sperm than eggs to be fertilized. This study models collective sperm movement as a diffusive search process, combining experiments and simulations to explore how heterogeneity in motility patterns and microenvironmental complexity shape fertilization success. We introduce simple metrics to quantify sperm fitness and the magnitude of selection pressure imposed by the microenvironment, revealing that sperm phenotype distributions interact with environmental constraints to determine the range of sperm traits that ultimately support successful egg contact. These insights improve our understanding of sperm population dynamics and offer practical tools for optimizing assisted reproductive technologies in clinical and agricultural settings.

Introduction

Assisted reproductive technologies (ARTs) are widely used in medicine and agriculture and include a variety of strategies such as *in vitro* fertilization, intra-uterine insemination, and embryo transplantation. Efficiency of ART is of utmost importance because of the implications for parental and offspring well-being, and significant time and cost investments. Though there are a multitude of factors that influence ART efficiency, one particularly salient challenge has been the pre-selection of sperm that have the potential to maximize the paternal contribution to the number and quality of viable embryos[1–3]. Identifying and isolating sperm with high fertility and developmental potential presents a significant challenge due to their structural and phenotypic heterogeneity, dynamic post-ejaculatory maturation processes, and the large quantity of cells in an ejaculate (i.e., order of 10^6-10^{11} depending upon species)[4–10].

Phenotypic variation in sperm has generally been explained by a game-theoretic competition model in which males adopt evolutionarily stable strategies that maximize fitness payoffs under sexual selection[11]. For example, mammalian sperm exhibit relatively high swimming velocity and/or greater sperm number per ejaculate in socioecological scenarios where there is strong between-male competition for mates[12]. Largely inspired by those observations, swimming velocity and sperm count have been regarded as heuristic guides for clinical sperm selection under the straightforward assumption that the ‘highest quality’ sperm can be identified from an idealized set of competitive traits[13].

However, heuristic approaches may be misleading because the predictions of sperm competition theory apply only to *between-male* variation, while *within-male* variation in sperm phenotype is the primary concern of assisted reproduction[11,14]. Importantly, male gamete function not only co-evolves with the competitive traits of other males, but also with the corresponding micro/macro-scale anatomy of the female reproductive tract. This effect, known as ‘cryptic female choice’, facilitates sperm selection in the reproductive microenvironment through various physical and chemical barriers (e.g., epithelial folds, cervical mucous, etc.)[15]. For example, mammalian sperm have evolved time-dependent changes in motility pattern (e.g., progressive to hyperactivated transition) that assist navigation of the labyrinth-like epithelial surfaces of the oviducts[16]. *Within-male* sperm selection may be an important component of mammalian reproduction and is a powerful candidate for the improvement of ART outcomes. However, our understanding of sperm selection at the cell population scale remains limited, and

there is currently no underlying theory that enables precise description of the key aspects of sperm selection - including a quantitative definition of sperm 'fitness', or a measure of the magnitude of selective pressure acting on sperm traits under a given set of conditions.

In this report, we investigate sperm selection as a consequence of the interaction between phenotypic variation among sperm populations and the constraints imposed on sperm fitness by the reproductive microenvironment. We use empirical data to inform the development of agent-based computational models (ABMs) and simulate 'bottom up' sperm population dynamics. We then extend concepts from probability and information theory to define a quantitative measure of sperm fitness (i.e., the posterior probability distribution of 'successful' traits obtained using Bayes theorem), as well as a measure of the magnitude of selection imposed on a sperm population during fertilization (i.e., the relative information gain). The results from this work lay a foundation for high-precision male fertility diagnostics to improve sperm classification and/or selection in conjunction with existing semen analysis and laboratory pre-selection procedures.

Results

Sperm-Agent Search is a Function of Ensemble Motility Pattern - We performed simulations and sensitivity analysis to investigate the relationships between motility pattern and the amount of discrete space searched in a bounded environment. Each simulation was performed with agents of only one motility type (progressive, intermediate, hyperactive, slow, weak, or mixed in equal proportions). Sperm began in a randomized position in the environment with the same total number in each simulation (N=250). The environment consisted of an underlying grid of 40 x 40 µm unit squares. Each grid square was considered distinctly 'searched' if at least one sperm passed through it. Simulations ended after two seconds, a typical time window for computer aided sperm motility analysis (CASA). The time color-coded movement paths of a representative simulation with 'mixed' sperm motility types is shown (Figure 1A). Populations of sperm with mixed motility types exhibited average movement patterns and an ability to search space that was reflective of the proportions of different motility types in the population (Figure 1B,C). These results demonstrate that the *average* search capability of a sperm population reflects the underlying *distribution* of sperm motility phenotypes. Notably, there are important mathematical properties exhibited by correlated random walks that may be useful for improving sperm motility analysis and fertilization more broadly (see the discussion section for more details).

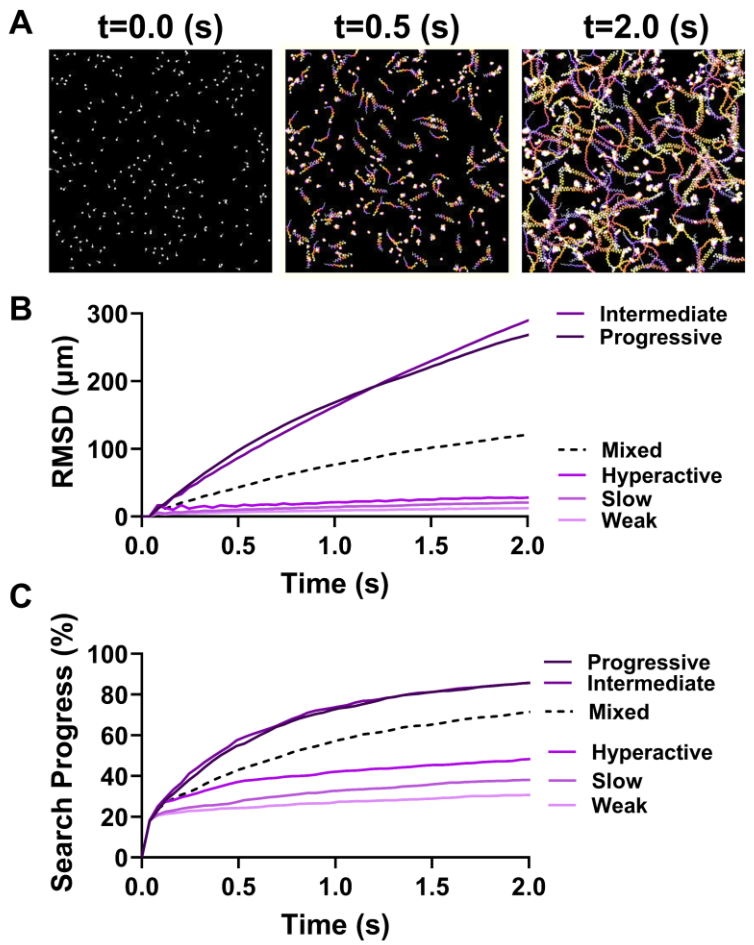

Figure 1: Sperm-Agent Search is a Function of Ensemble Motility Pattern. (A) Representative model simulation of 250 sperm with equal proportions of each motility type searching a closed space. Color scale is blue (early) to white (late) frames in the video. (B) Root mean squared displacement (µm) for simulations involving the indicated composition of motility types. Mixed populations consisted of 50 sperm of each motility type. (C) Search progress (%) for the simulations described in subpanel (B).

Sperm number and search properties - To explore the relationship between sperm-agent number (or density within the simulation space) and search in complex spatial microenvironments, simulations were performed for increasing numbers of sperm (1-10^4 progressively motile sperm; 100 simulations each). The simulations ended when the egg was contacted for the first time by one of the sperm (Figure 2A; top- TC_w =1; middle- TC_w = 22; bottom- TC_w = 54)**.** Notably, the time to first contact was not symmetrically distributed for each sperm-agent density, which became symmetric when placed on a logarithmic scale. Simulations involving 10^3 and 10^4 sperm became much more likely to be normally distributed rather than lognormally distributed in Mazes B and C, but not A. However, tests for lognormality were inconclusive and it is not clear what the underlying distributions were in either case, though it was clear that the distributions were skewed in simulations with fewer sperm (Figure 2A).

Next, we investigated the relative impact of environmental complexity on the efficiency of the search process by examining what quantity of the searchable area was accessed during each simulation (Figure 2B; top- TC_w =1; middle- TC_w = 22; bottom- TC_w = 54). We hypothesized that sperm ensembles would perform something like a depth-first search in which all preceding branches of the maze were likely to be searched prior to finding the egg[17]. Indeed, the sperm searched more space prior to finding the egg as the number of agents in the

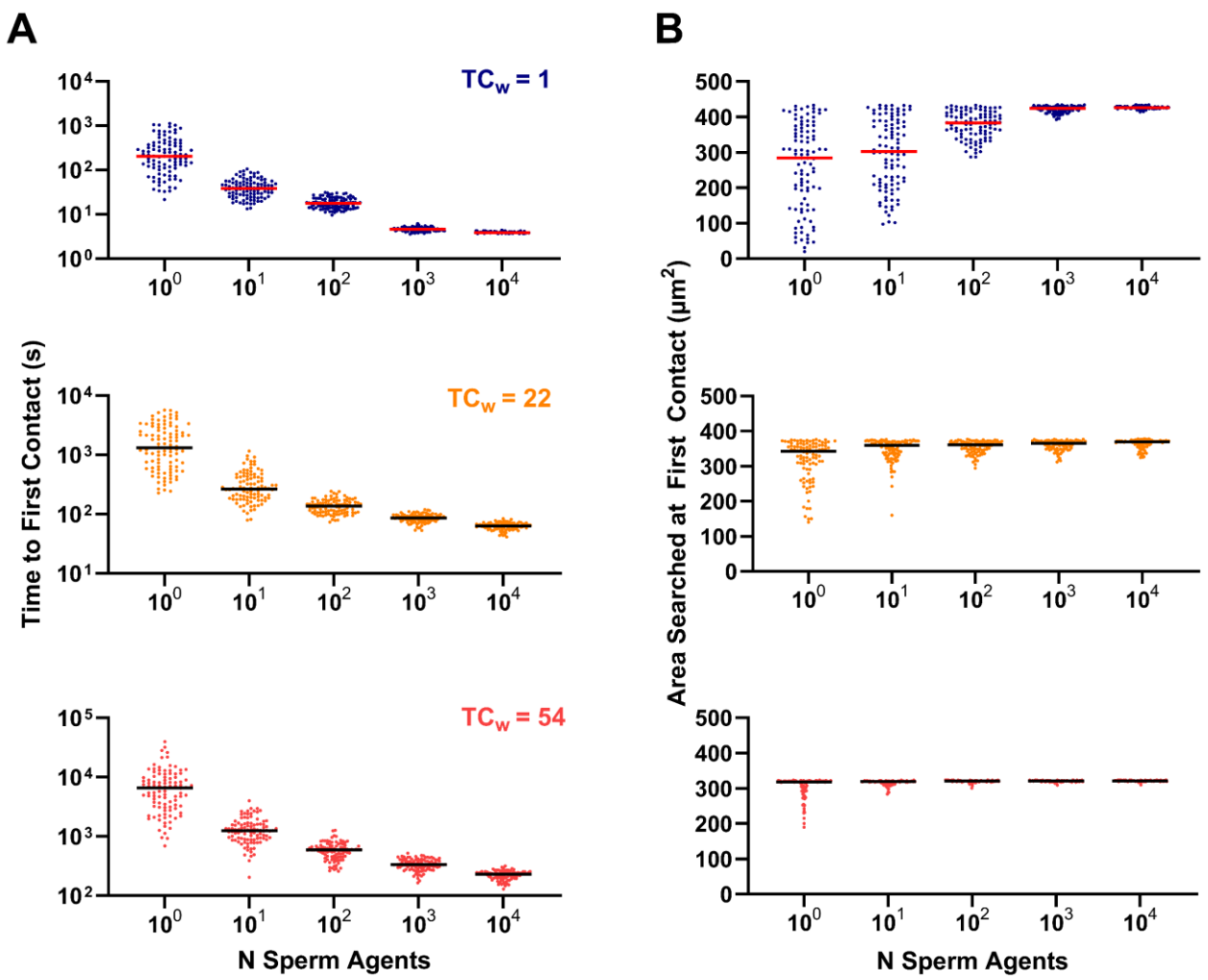

Figure 2: Sperm number and search properties. (A) Time to first contact with an egg in microenvironments with TCw=1 (maze A), TCw= 22(maze B), and TCw=54 (maze C). (B) Area (µm2) searched at first contact with the egg for microenvironments with increasing weighted complexity (top to bottom as in subpanel A). Lines indicate the median. N = 100 simulations for each condition.

simulations increased (Figure 2B). Interestingly, at low sperm number (< ~10^3), the role of chance was large compared to simulations with larger numbers of sperm, and in many cases the sperm were able to contact the egg without searching a large proportion of the space. This effect was particularly relevant in the open environment of maze A, but was diminished with increasing environmental complexity in mazes B and C.

Taken together, these results predict that diffusive search by non-adaptive sperm will exhibit a non-linear relationship with sperm density and that the role of chance in finding shortest path to the egg is modified by the spatial complexity of the microenvironment. As the microenvironment becomes more complex, more sperm are required to minimize the time to egg contact, but the benefit gained by increasing sperm number above a critical

threshold also diminishes nonlinearly due to convergence on the most direct path to the egg. These insights may provide a basis for optimal prediction of sperm number for ART procedures such as IVF, though these models do not explicitly account for the risk of polyspermy which would likely form an upper bound on sperm density due to decreasing zygote fitness with increased risk of polyspermy. Additionally, there are several useful mathematical properties that describe the asymptotic behaviors of persistent random walks in mazes that may inform sperm motility analysis and the physiology of fertilization more broadly (see the 'random walks' subsection the discussion for more details).

A time homogeneous Markov model of sperm phenotype heterogeneity - Individual sperm undergo dynamic changes that are conditioned on nutrients and signaling factors in the microenvironment. These factors ultimately influence sperm behavior, lifespan, and ability to recognize and bind to an egg[5,18–21]. In mammalian sperm, intracellular calcium is a key second messenger that mediates capacitive changes, and heterogeneity in calcium transients are a key source of individual sperm variation within cell populations[9,22]. To aid in choosing parameter distributions for the agent-based models, we explored the effect of natural variation in isolated mouse cauda epididymal sperm in response to well-defined capacitive signaling inputs (Figure 3). To account for the controlling effect of exogenous free calcium, we performed simultaneous pseudo-titrations of total calcium using an ethylene glycol-bis(β-aminoethyl ether)-N,N,N′,N′-tetraacetic acid (EGTA) chemical 'clamp' system to buffer the free calcium at defined concentrations (Figure 3A). We then combined this method with pseudo-titrations of sodium bicarbonate (HCO_3^-), a key signaling factor that stimulates capacitation via activation of soluble adenylate kinase. Intracellular calcium was monitored using an acetoxy-methyl ester Indo-1 (ratiometric) dye. HCO_3^- stimulated intracellular calcium increase concomitant with exogenous free calcium concentration over a period of two hours (Figure 3B). These measurements highlight the average responses that sperm populations make to signaling inputs.

Next, we sought to determine how intracellular calcium was distributed among individual sperm at the 60-minute timepoint using spectral flow cytometry, with a similar multi-dimensional culture array scheme (Figure 3C). Examination of the qualitative distributions of intracellular calcium ($[Ca^{2+}]_i$ with increasing concentrations of HCO_3^- revealed that $[Ca^{2+}]_i$ exhibited a positively skewed distribution. We interpreted the skewed shape of this

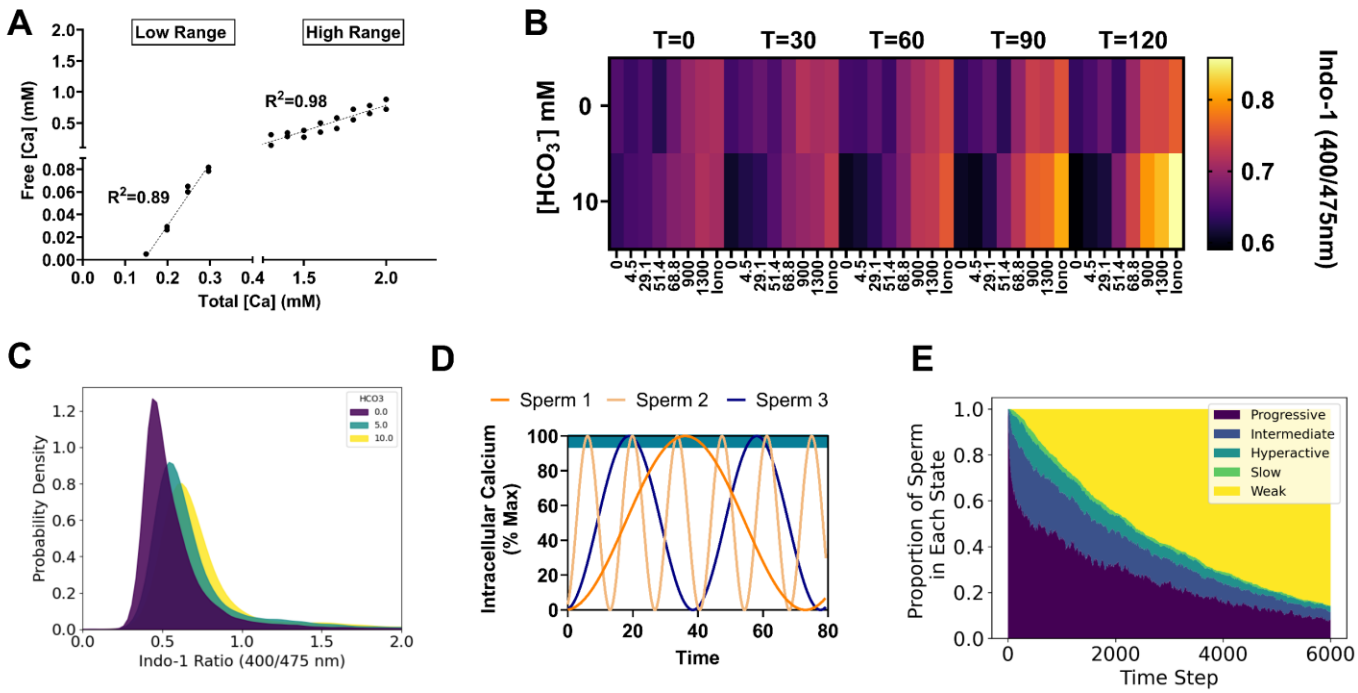

Figure 3: A Time-Homogeneous Markov Model of Sperm Phenotype Heterogeneity: (A) Linear regression curves for different calcium ion selective electrode filling solutions used to calculate the free Ca2+ concentrations in HEPES buffered assay media in the presence of 1mM EGTA. (B) Representative heat map showing Indo-1 fluorescence ratios for sperm under the indicated Ca2+ and HCO3- pseudo-titration conditions. Iono = ionomycin. Free calcium concentrations (bottom) are in micromolar units. T = time since the beginning of the assay in minutes. (C) Probability density estimate from spectral flow cytometry for approximately 105 live cells per indicated condition. Dead cells were excluded from analysis based on ToPro3 fluorescence intensity. (D) Representative intracellular calcium oscillations derived from a squared sine function assigned to each sperm in the model simulations. Teal bar at the top of the graph indicates the upper 5% of the concentration range during which the cells were allowed to transition motility states according to a Markov probability transition table. (E) Relative proportion of sperm in each indicated motility state over time (in model-timestep units). In the long run, sperm in the models absorbed into a weak motility state.

distribution as an indication that high $[Ca^{2+}]_i$ cells are a relatively 'rare' phenotype relative to the mean, a pattern which was invariant to the magnitude of the HCO_3^- signal.

To facilitate modeling physiological changes in motility phenotype over time, the sperm in the agent-based models were updated to include a 'calcium oscillator' function that influences the behavior of the sperm in proportion to the 'frequency' of intracellular calcium transients (Figure 3D). We associated the following equation with each agent in the simulation:

$$[Ca^{2+}]_i = \frac{1}{2}(1 - \cos \Omega_i t)$$

Each cell was assigned a randomly generated oscillation frequency Ω_i, drawn from a Poisson distribution. Use of the Poisson distribution was motivated by the skewed indo-1 fluorescence ratio distributions observed in the flow cytometry measurements of intracellular calcium distributions. It describes the probability of observing a given Ω_i for an interval of discrete oscillation frequencies with mean (λ) and has the property that the sequence of inter-frequency intervals between sperm subgroups will be independent and exponentially distributed with mean $(1 / \lambda)$. To model changing population states over time, all sperm began with a progressive motility state and were allowed to change motility states when the intracellular calcium was above $[Ca^{2+}]_i > 0.97\%$ of the maximum. The changes were stochastic, following a time-homogeneous Markov model. Motility patterns (i.e., progressive, intermediate, hyperactive, slow, and weak) were assigned using a probability transition table (S2 Table). Since the weak mobility state was final and could not be left once reached by a given sperm, the population experienced a net flow towards this state over a long run period, similar to overall motility degradation observed in live sperm samples (Figure 3E). Overall, this logic models the empirically measured effects of intracellular calcium oscillations on the motility state distributions of sperm [9,22,65], and simulates natural (stochastic) variation in the rates at which individual sperm undergo capacitation.

A Poisson-distributed calcium oscillation frequency with a mean (λ) of 1 Hz results in most sperm exhibiting low-frequency oscillations, with a few 'rare variants' exhibiting higher oscillation frequencies. The effect of selection (conditioning on the microenvironment) on sperm populations can be explored by comparing distributions with different means, or incorporating different phenotype distributions altogether (i.e., Gaussian, exponential, etc). These distributions take on important meaning in the context of overall fitness of the sperm population and facilitate exploration of how sperm phenotype distributions impact the aggregate fitness of sperm populations.

Impact of phenotype heterogeneity on diffusive search- Using the empirical findings to inform model updates incorporating motility phenotype distributions, we then simulated search for an egg in microenvironments with increasing spatial complexity (Figure 4). Simulations consisted of 100 sperm, which was chosen as a reasonable (minimal) number that supported consistent random phenotype distributions across simulation runs, determined by increasing the size of sampled distributions until the observed mean approximately matched the ideal mean of the distribution from which the sample was drawn. A two-factor design was implemented to compare the relative effects of sperm population heterogeneity (mean calcium oscillation frequency; λ) and

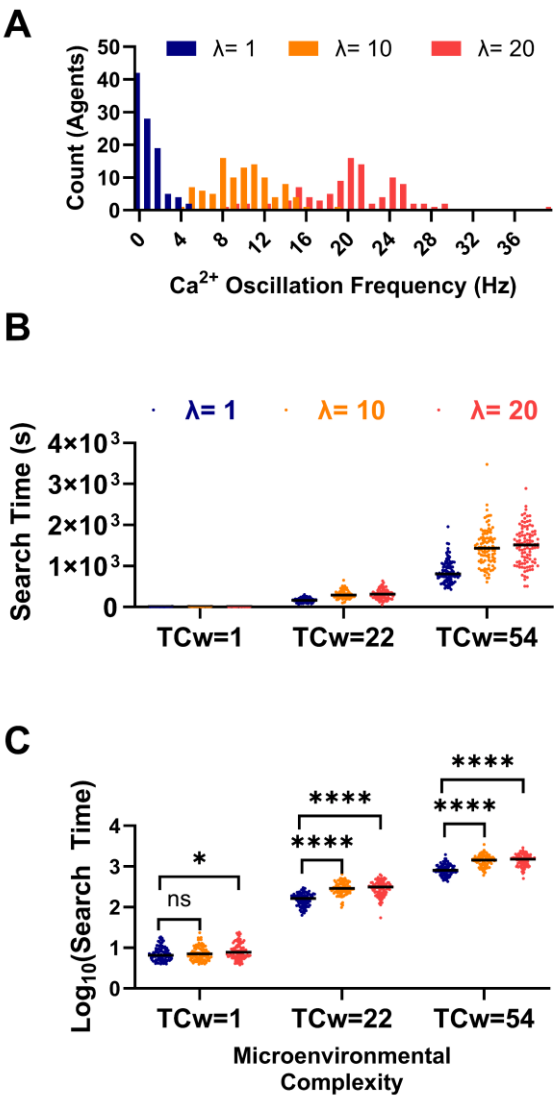

Figure 4: Impact of Sperm Phenotype Heterogeneity on Diffusive Search. (A) Histogram of the sperm intracellular calcium oscillation frequencies randomly drawn from a Poisson distribution with the indicated means (λ). (B) Search time for sperm populations with different phenotype distributions in microenvironments with increasing total weighed complexity (TCw). (C) Logarithmically transformed search times from subplot B used for statistical analysis to satisfy 2-way ANOVA assumptions. Ns = not significant, *p<0.05, ****p<0.0001. Lines indicate medians. Simulations consisted of N = 100 agents.

microenvironmental complexity (TC_w) on search time. Intracellular Calcium oscillation frequencies assigned to each sperm were drawn from one of three Poisson distributions characterized by different means/variances (λ) (Figure 4A). A low λ value indicates that most of the sperm had low Calcium oscillation frequencies, and thus, would absorb into a weak motility state slowly, giving them more time to actively search for the egg. Conversely, a high oscillation frequency might absorb into a weakly motile state quickly, making it less likely to find the egg by comparison.

A plot of search time vs. TC_w for each value of λ qualitatively indicated that both microenvironmental complexity and phenotypic heterogeneity influenced the search time (Figure 4B). Due to the asymmetry of the search time distributions, the assumptions of a two-way ANOVA were not met. To address this issue, we performed a two-way ANOVA on logarithmically transformed search time (Figure 4C), and a statistically significant interaction was detected between TC_w and λ ($F(4, 891) = 22.41$; $P<0.0001$); however, the effect only accounted for 0.29% of total variation. Simple main effects analysis revealed that λ accounted for only 0.82% of variation ($F(2, 891) = 127.6$; $P<0.0001$), while TC_w accounted for most of the variation (95.99%; $F(2, 891) = 14808$; $P<0.0001$). Post hoc analysis using a Tukey's multiple comparison test indicated statistically significant differences between the λ levels in all three microenvironments with mean search time differences as

large as ~627 seconds in the most extreme case (TC_w=54; λ=1 Hz Vs. λ=20 Hz). Together these simulation outcomes predict that both phenotypic heterogeneity and microenvironmental constraints interact to impose selective pressure on fertilizing sperm. An important remaining question is how to quantify both the impact and magnitude of selection on sperm fitness.

Environmental complexity narrows the posterior distribution of fit sperm- Further exploration of the interaction between sperm-agent population dynamics, spatial constraint, and the effect of selection requires measures of how the distribution of sperm phenotypes changes under selection as well as the magnitude of effect caused by the selective pressure. We considered two measures that have been used in similar biological contexts to model changing phenotype distributions among populations 1.) Bayesian inference - the posterior probability of contact with an egg given that a sperm has a particular Calcium oscillation frequency, and 2.) Kullback-Leibler divergence (a.k.a. relative information gain) - an information theoretic measure of the *magnitude of effect* of selection on the distribution of Calcium oscillation frequencies following diffusive search in microenvironments with differing degrees of complexity. These approaches especially useful in this context because they are non-parametric and are easily interpreted even when the sample size is small, which is relevant given that only a few sperm may ultimately gain access to the egg during fertilization.

The posterior distribution provides a quantitative measure of sperm fitness - For these simulations, the agent-based models were updated to facilitate tracking the number, assignment, and duration of contact time with the egg by each of the sperm. A total contact-time threshold of five seconds was defined as a condition to end the simulations. The underlying assumption was that after a threshold value for contacts by one or more sperm, the fertilization process is likely to have occurred if it will occur at all. As in the previous sections, 100 simulations involving 100 sperm were carried out for each factor and corresponding level (i.e., {λ: λ = 1, 10, 20 Hz}, and {TC_w : TC_w = 1, 22, 54}) (Figure 5). The relative proportion of the ith Calcium oscillation frequency is denoted q_i. To visualize the initial distributions across the λ and TC_w levels, cumulative probability distributions were calculated, demonstrating approximately identical initial distributions across the simulations (Figure 5A).

The distribution of each discrete Calcium oscillation frequency among the sperm that contacted the egg is also known as the likelihood function $P(q_i \mid contact)$. Plotting the likelihood function vs. each distinct Calcium oscillation

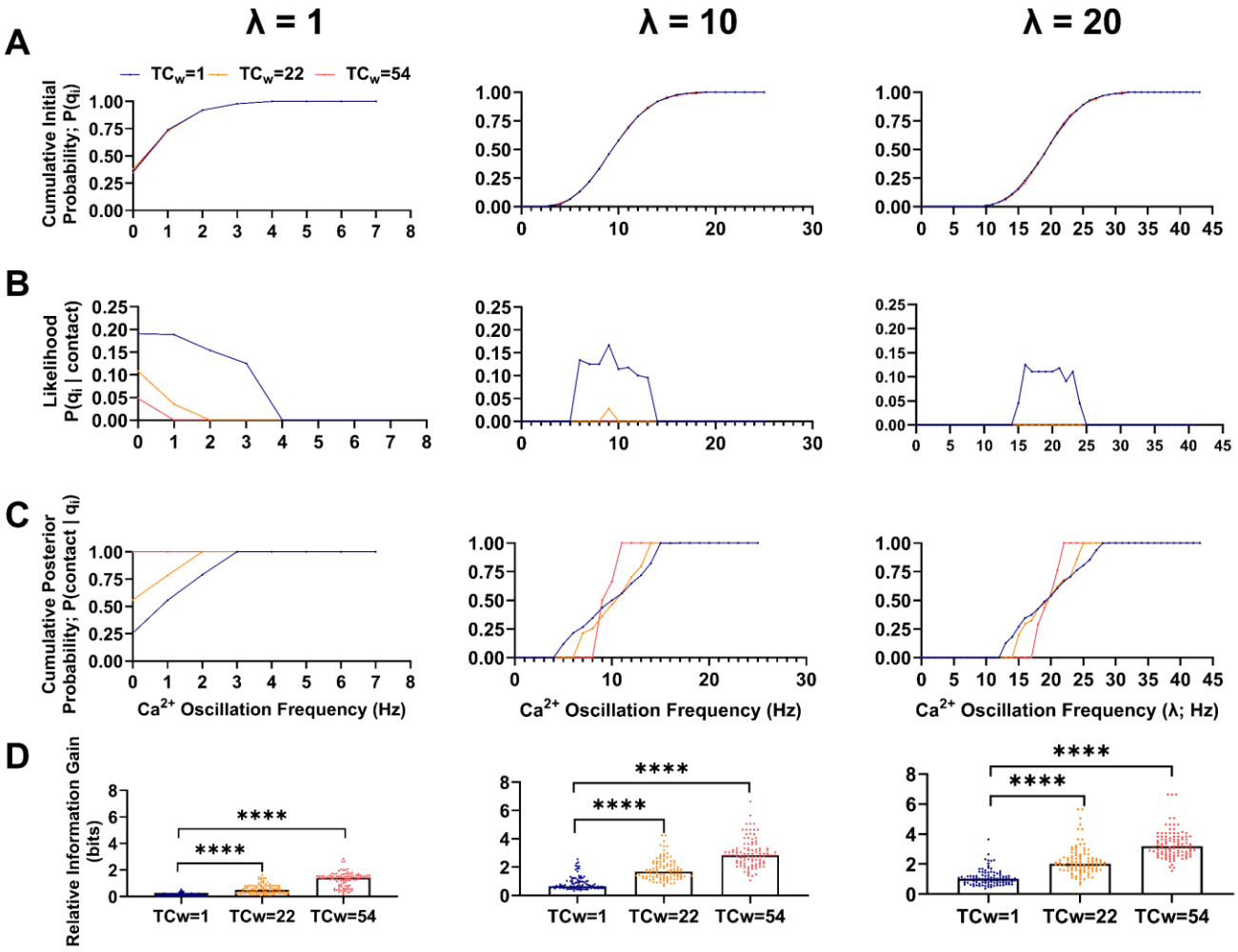

Figure 5: Measures to Infer Sperm 'Fitness' as well as Quantify the Magnitude of Sperm Selection. (A) Cumulative distributions total probability P(qi) for each oscillation frequency in the initial sperm population for each simulation condition. (B) The Bayesian likelihood (frequency of sperm for each oscillation frequency that contacted the egg). (C) Cumulative posterior probability of egg contact for each oscillation frequency. Note, a prior distribution of 1/N, where N is the total number of sperm in the simulation, was used in the calculation. This can be interpreted to mean that each sperm had an assumed equal chance of contacting the egg. (D) Relative information gain (a.k.a. Kullback-Leibler divergence) calculated for each simulation condition. ****p<0.0001. TCw = total weighted complexity. N = 100 sperm in each simulation. Points in A-C represent the median of 100 simulations. Points in D represent relative information gain for each of 100 simulations.

frequency indicated that increasing environmental complexity narrowed the range of frequencies among sperm that successfully made contact (Figure 5B). It also reduced the absolute number of unique sperm that made contact. Though the likelihood function is the typical empirical measure used in laboratory experiments related to sperm fertility competence, it lacks information about prior assumptions regarding the fitness of sperm traits as well as the phenotype distribution of those traits within the initial sperm population (before fertilization

outcomes are known). In other words, the likelihood function is a *sampling* distribution, but what we are most interested in is the *inferential* (posterior) distribution, which can be obtained using Bayes theorem:

$$P(contact \mid q_i) = \frac{Prior * Likelihood}{Total\ Probability} = \frac{P(contact)\, P(q_i \mid contact)}{P(q_i)}$$

where $P(contact)$ is the hypothesized prior distribution, in this report $P(contact) = \frac{1}{N}$, where N is the total number of sperm in the simulation. $P(contact)$ can be interpreted to mean that all sperm were assumed to have an equal chance of contacting the egg (prior to observing the outcome). Calculating the posterior distribution in this way addresses the question- "what is the probability that a given sperm will be 'successful' given that is has a particular trait value". Cumulative posterior probabilities were calculated for each level of TC_w and λ (Figure 5C). Interestingly, the range of successful oscillation frequency values was narrowed by increasing microenvironmental complexity, enabling identification of a subset of sperm that could be considered to have high 'fitness' within each microenvironment.

Quantifying the magnitude of selection imposed by the microenvironment- Sperm selection is often used in ART applications, but the magnitude of selective effect is generally not considered, despite the importance of such a measure for comparing the effectiveness of different selection strategies. Here we describe use of relative information gain as measure of the magnitude of selection. As in the previous section, q_i is the initial distribution of sperm-agent Calcium oscillation frequencies. Let q_i' denote trait probabilities among the proper subset of sperm that successfully made contact with the egg. If q_i and q_i' are the same, then there was no selection for Calcium oscillation frequency during the simulation. However, if q_i and q_i' are not the same distribution, then some subset of Calcium oscillation frequencies did not contact the egg, implying they were selected against by the conditions of the simulation. The normalized distance between the two distributions can be quantified with the following expression:

$$D(q' \,||\, q) = \sum_{i=1}^{n} q_i' \, log_2\left(\frac{q_i'}{q_i}\right)$$

This expression is known as the relative information gain (or Kullback-Leibler divergence), and its units are in binary digits (bits). A relative information gain of 0 indicates the distributions are the same, and a positive number indicates the magnitude of the difference between the two distributions. The relative information gain cannot be

less than 0 and this measure is not symmetric, meaning that it is not equivalent to $D(q \,//\, q')$. As anticipated, increasing TC_w or λ increased the relative information gain (Figure 5D). Two-way analysis of variance (ANOVA) revealed a statistically significant interaction effect among TC_w and λ ($F(4, 891) = 19.47$; $P<0.0001$), which only accounted for ~2% of the total variation. Simple main effects analysis indicated that TC_w accounted for about 37% of the variation ($F(2, 891) = 542.9$; $P<0.0001$) and λ accounted for about 29% ($F(2, 891) = 425.9$; $P< 0.0001$). The results of a Tukey's post hoc test comparing each λ level to λ=1 are indicated in (Figure 5D).

Taken together, the results from these simulations reinforce the conclusion that simple spatial hindrance by the latent structure of the microenvironment combined with variation in individual sperm phenotypes exerts quantifiable selective pressure on sperm during fertilization. The proposed measures enable quantitative description of sperm fitness and the magnitude of selection in relatively simple terms.

Discussion

Random walks - The asymptotic properties of diffusive and correlated random walks have been well studied and described previously[23]. The goal of this report is not necessarily to derive new findings on random walk behavior, but rather, to frame the physiological context of the sperm search for an egg using tools from this field with the hope of illuminating improved fertility analysis and/or prediction. General random walk models, similar to those presented in this report, have several notable properties- 1) First passage probabilities, akin to the probability that a sperm will find an egg, are heavily influenced by dimensionality[24], 2) correlation among successive steps (i.e., persistence of the walkers), akin to progressive sperm motility patterns, produces scaling properties that are distinct from uncorrelated random walks[24], 3) the number of distinct sites visited by a given number of random walkers, akin to how sperm explore space, has been shown to exhibit distinct time regimes that depend on the system size (i.e., the area of the environment and the number of random walkers)[25] and finally, 4) random walks on undirected graphs, akin to sperm movement in the epithelial folds of the uterus and oviducts, exhibit polynomial traversal times- bounded above by $T \leq 2e(n-1)$, where e is the number of edges and n is the number of nodes[17]. Together, these properties may be extended to inform the behavior of diverse sperm populations searching in spatially complex microenvironments.

A systems perspective on fertilization **-** The molecular mechanisms that underpin the regulation of mammalian sperm post-ejaculatory maturation (a.k.a., capacitation) have been thoroughly studied, and consist of signaling pathways[20,26], metabolic processes[18,19,27], and complementary binding of cell surface molecules[28,29]. Though there are excellent physical models of individual sperm motility function and regulation[16,30–34], few models account for the stochasticity of hundreds of millions of sperm searching for an egg that ultimately determine fertility outcomes; this gap in knowledge persists despite consistent observations of significant phenotypic heterogeneity within sperm populations (e.g., the localized expression of ion channels on the plasma membrane) [4,6,9,35].

Previous work modeling sperm search times in both 2D and 3D environments detailed several potential scaling laws for the diffusive search process relating search time to sperm number[36]. Similar to our observations in this report, a non-linear relationship between sperm number and search time was described, and the scaling relationships depended on the dimensions of the search space. However, those simulations used sperm with constant velocity, rectilinear motion, and did not explicitly account for phenotypic heterogeneity or motility pattern changes over time. The agent-based models (ABMs) developed in this report are informed by empirical data and provide a structured framework to explore the complex collective dynamics of phenotypically heterogeneous sperm populations under various environmental conditions. The models facilitate a deeper understanding of the interactions between microenvironmental complexity and sperm phenotypic heterogeneity, emphasizing the stochastic nature of the variables that shape sperm fitness.

Diffusive search under microenvironmental constraint - The spatial scale of motility is important when analyzing the consequences of motility pattern distributions on sperm selection. *In vivo*, peristaltic fluid flow moves sperm suspensions over relatively large distances within the female reproductive tract independent of their motility status[37]. Though this phenomenon will distribute the cells on a macroscopic scale, at the microscopic scale, individual sperm must still ‘search’ local space using flagellar movement in a manner that increases probability of contact with the egg. This important property implies that critical cellular density thresholds, cell intrinsic motility characteristics, and microenvironmental factors such as physical/chemical barriers play critical roles in influencing which sperm from a given cell population will have an opportunity to fertilize. The degree to which this is due to chance alone is an important consideration, and a theoretical framework for sperm selection should

account for the probabilistic dependencies of sperm fitness. The simulations in this report predict that increased microenvironmental complexity requires greater sperm density to maintain effective diffusive search and timely egg contact, highlighting potential tradeoffs between the collective diffusive search capability of a sperm population and the number of required sperm. The models also predict that critical thresholds exist, above which sperm number plays a diminishing role in diffusive search capability. Importantly, this threshold is not a fixed value, but rather, depends on the complexity of the microenvironment and the phenotypic heterogeneity of the sperm population.

Impact of sperm phenotypic heterogeneity - Motility is the most fundamental physiological function of mammalian sperm and is a common distinguishing feature used in clinical sperm selection[38,39]. Our results demonstrate how intrinsic phenotypes of sperm, such as intracellular ion transients coupled with the regulation of motility pattern, may critically influence selection outcomes. Sperm phenotypic variation is complex and caused by many different factors. Variation may be an important driver of optimal sperm number among (or within) species, based on the observation that sperm number is positively correlated with potentially deleterious effects of genomic recombination during meiosis[40]. Variation may also be undergirded by an evolutionarily stable strategy that optimizes the number of capacitated sperm during a post-copulatory fertilization window; a process facilitated by periodic synchronous capacitation among sperm subpopulations[41]. Regardless of the underlying causes of variation, the simulations in this report suggest that the reproductive microenvironment is a critical factor in sperm selection because it ultimately determines which sperm phenotypes will have access the egg. This suggests that sperm selection protocols for ART should consider both the statistical distribution of biological variability among the sperm and the physical/chemical structure of the microenvironment in which fertilization will occur.

Quantifying sperm fitness and selection pressures - Sperm pre-selection is almost ubiquitous in routine clinical diagnostics and ART procedures (e.g., gradient centrifugation, swim-up assays, hyaluronan binding assays, etc.). Though semen parameters such as motility and sperm count are known to influence ART outcomes[42], current methods of selection largely depend on simple *correlation* and qualitative assumptions about the effects of selection[43]. Additionally, use of ICSI has increased substantially in recent decades, a procedure which relies on direct selection of a single sperm for injection into the egg[44]. Currently, there is no quantitative framework

that facilitates high-precision sperm selection from *within-male* samples and sperm 'fitness' remains nebulously defined.

Though fitness could be quantitatively framed in many ways - Bayesian inference is a particularly useful approach because it is insensitive to the base rate representation of sperm phenotypes and has no minimum sample size. The approach taken here is drawn from the theory of natural selection, in which fitness is defined as a probability measure of success[45], which has classically been defined by survival or reproduction of organisms within a given population. For the purposes of modeling fertilization, success can be defined flexibly depending on the scenario without altering the underlying mathematical representation (e.g., egg contact, fertilization, passage through a selective barrier, etc). Most approaches to assessing sperm fitness are based on regression of sperm traits (or interventions) with fertility or developmental outcomes[46,47]. However, it is important to consider that the probability that a sperm has a particular trait given that it fertilized an egg, is not necessarily equivalent to the probability that a sperm *will fertilize* an egg given that it has a particular trait, though it is the latter condition (inference) that is of prime interest for sperm selection in ART.

Bayes theorem incorporates useful information beyond simple sampling frequencies. For example, it accounts for the relative proportion of sperm with 'successful' sperm traits in the initial population and prior information about the traits' contributions to fertilizing potential. Bayesian inference has been used recently in conjunction with dimensionality reduction to make fertility predictions from motility stereotypes in boar semen[48]. Quantitatively defining sperm fitness is becoming more important as machine learning and computer vision technologies advance, allowing for high-dimensional data collection from semen samples, and necessitating methods that analyze distributions directly rather than relying on summary statistics[49]. One advantage of the approach taken in this report is the computational simplicity, which may be useful for developing classification or selection strategies that rely on interactive microscopy video manipulation in real-time.

Another major limitation to improving current male fertility diagnostics and high-precision selection is that fertilization is an open-ended process, making it very difficult to predict which sperm will have a selective advantage from semen analysis alone. As mentioned previously, the microenvironment plays a substantial role in constraining which sperm will have access to the egg. For this reason, it is critical to have some measure that can compare between the selective effects introduced by different reproductive microenvironments *in vivo* or *in*

vitro. To address this limitation, we propose another measure - relative information gain - for quantification of the magnitude of selection imposed by the reproductive microenvironment[45]. This measure, also known as Kullback-Leibler divergence, provides a useful way to compare selection strategies quantitatively[50]. It is a numerical representation of the 'distance' between the trait distribution of an initial (pre-fertilization) population of sperm and the 'successful' (post-fertilization) population of sperm. Notably, it is independent of the actual features of the microenvironment and is only dependent on the effect of microenvironmental constraint on sperm fitness. Additionally, it lays the groundwork for a new biological context for reproduction by reframing the process of fertilization in information theoretic terms as a form of learning process[51].

Model Limitations- There are several notable limitations of the models developed in this report. Most of the limitations stem from the simplifying assumptions made about the physiological phenomena that underly mammalian reproduction. First, the sperm movement functions are relatively simple, but real sperm exhibit more complicated patterns such as helical progression[52]. Second, the regulatory systems in the model that control the timing and trajectory of capacitation are limited only to calcium transients with an assumed correlation between intracellular calcium concentrations and motility pattern transitions. This simplification ignores a much more complicated reality involving time-inhomogeneous plasma membrane potassium hyperpolarization, metabolic energy balance, protein tyrosine phosphorylation, and other key biochemical reactions. Though the results should be interpreted with caution, the models were designed to capture key elements of cell population scale dynamics and were constrained by empirical data to enhance their physiological relevance. These models may be extended to incorporate updated movement parameters and regulatory subsystems - for example through use of coarse-grain approaches such as Boolean networks or more involved systems of differential equations[9,53]. Finally, to approach this problem in a general way, we modeled only *non-adaptive* sperm, meaning sperm that do not change their motility pattern in response to environmental inputs. However, there are many ways by which mammalian sperm modulate behavior in response to their environment including chemotaxis, rheotaxis, and thermotaxis. Incorporating these behaviors will likely affect the statistical predictions about sperm fitness and should be pursued in future studies.

Materials and Methods

Model implementation - Agent-based models were developed and implemented using the Netlogo modeling environment (V6.2.2)[54]. Netlogo BehaviorSpace was used for repeated simulations with parameter scaling. The models and other supporting information are available at (https://github.com/cas-mitolab/Fertilization_ABM). Simulations were run on a standard laptop computer with 16 GB of RAM and an Intel Core i7 1.7GHz processor. Markov state transition simulations and calculations related to Bayesian inference and relative information gain (Kullback-Leibler divergence) were performed using the Python (V3.9) programming language and the NumPy library (https://github.com/cas-mitolab/Fertilization_ABM)[55].

Model aim and context- The models are meant to simulate physiologically relevant aspects of sperm motility that contribute to sperm selection under microenvironmental constraints. The core models were designed using simple self-propelled particle physics, similar to the methods used in Computer Aided Sperm Motility Analysis (CASA), in which motility measures are obtained by digitally locating, annotating, tracking, and summarizing the trajectories of sperm nuclei in microscopy videos[56]. The models were fit to empirical data to improve accuracy and physiological relevance.

System boundaries- The physical environment simulated by the models approximates a 10X field-of-view under a light microscope with 680 X 680 μm side lengths and approximately 4.62×10^5 μm^2 area (S1 Figure A). Sperm motility imaging is typically performed using ~20 μm depth chambered slides that restrict the axial mobility of the cells for the study of 'planar' flagellar beating[57]. Although the models are 2D, they can be considered to have a 3D quality because the sperm are allowed to freely cross paths, as would occur in depth-chambered slides. The environment is comprised of a regular grid-space arranged in four quadrants. The grid squares were assigned a length scale value chosen to facilitate accurate approximation of empirically derived microscopy data (40 μm for the dimensions described above)[58]. The length scale factor can be adjusted to facilitate modeling any spatially defined environment. A separate agent-based model was designed to facilitate drawing and saving the environment (available at https://github.com/cas-mitolab/Fertilization_ABM). White barriers are imposed in the model as boundaries that sperm cannot cross, simulating the physical and physiological barriers that constraint sperm motility in the female reproductive tract. These maze-like environments can be customized using the drawing model mentioned above.

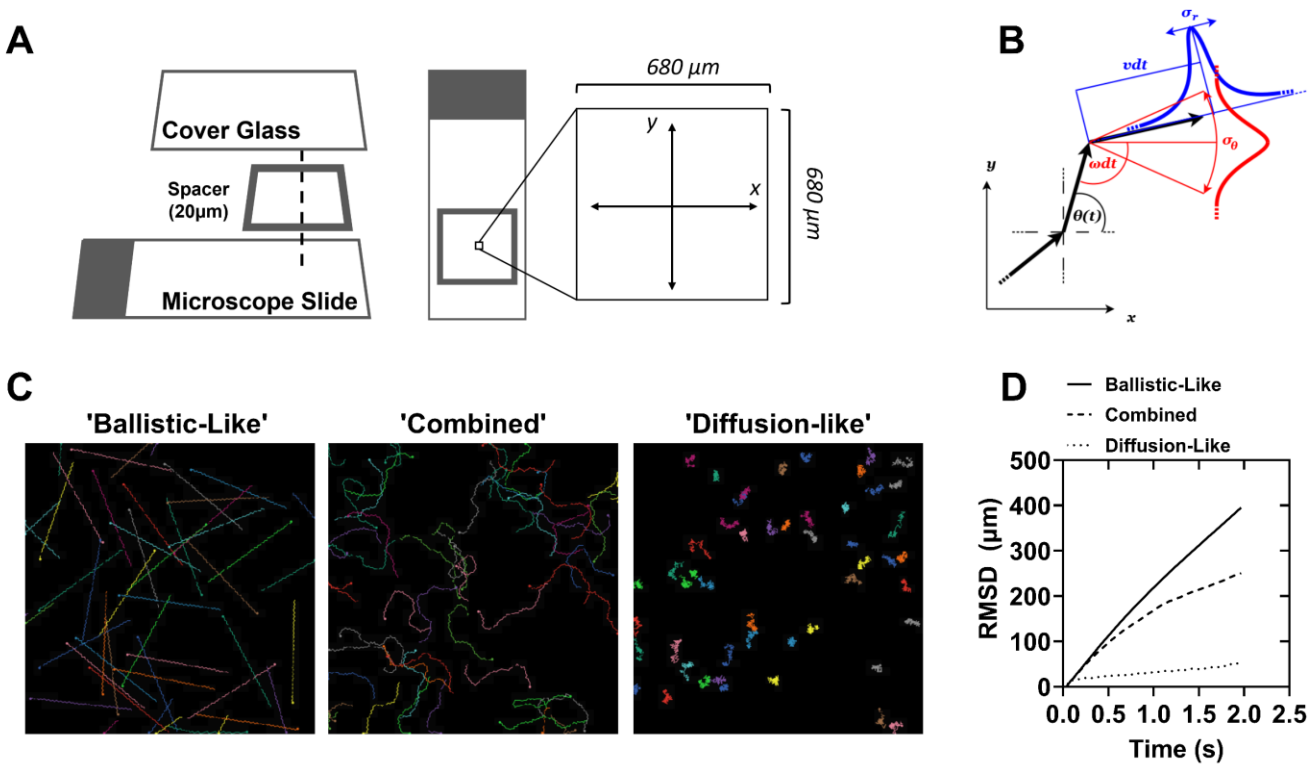

S1 Figure: Simulated random walkers explore space in a manner that depends on their movement properties. (A) Diagram of the model environment, which is designed to emulate an isolated portion of the field of view of a light microscope with a 10X objective and a 20 μm deep chambered glass microscope slide. (B) Diagram of the core movement functions employed by the agent-based model. Θ(t) is the angular rate of change, v(t) is the radial rate of change, σ is the respective amplitudes of zero average Gaussian noise added to the parameters. (C) Example images of simulations highlighting extremes of model behavior based on the choice of parameters. Ballistic-like motion results from no Gaussian noise being added to the radial and angular velocities; Combined motion results from combinations of the radial and angular velocities as well as the amplitude of noise added to each term; Diffusion-like motion results from relatively large values of noise amplitude. (D) Root mean square displacement of simulations with 50 agents as a measure of the relative distance traveled by the particles on average from their point of origin after 50 steps. Colors are randomly assigned to the agents and serve to facilitate distinguishing the trajectories only.

Core Movement Functions - The agent-based models in this report were designed to simulate sperm motility in an experimentally tractable setting- i.e., a typical 20 μm depth-chambered slide, like those used in standard computer aided sperm motility analysis (CASA). A diagram of the modeling environment is shown (S1 Figure A). The agents in the simulations represent the spermatozoon nucleus, in the same manner that sperm nuclei are typically imaged, filtered, and tracked using phase contrast microscopy for 2D path reconstruction in CASA[56].

The agents in the simulations execute the self-propelling random walk (S1 Figure B). That is, each agent is characterized by its velocity vector $\vec{v}_i(t) = (\dot{x}_i(t), \dot{y}_i(t))$ and the angle $\theta_i(t)$ at which this velocity vector is

directed, subjected to random fluctuations. The components of $\vec{v}_i(t)$ and $\theta_i(t)$ obey the following equations of motion:

$$\dot{x}_i(t) = \cos\big(\theta(t)\big)\,[v + \sigma_r \eta_{r,i}(t)]$$

$$\dot{y}_i(t) = \sin\big(\theta(t)\big)\,\big[v + \sigma_r \eta_{r,i}(t)\big]$$

$$\dot{\theta}_i(t) = sgn(\sin(2\pi t/\tau))\big[\omega + \sigma_\theta \eta_{\theta,i}(t)\big]$$

Here, i numerates the agents, while $\eta_{r,i}(t)$ and $\eta_{\theta,i}(t)$ are the zero-average uncorrelated Gaussian noises and $sgn(\ldots)$ is the signum function. When random fluctuations are not present ($\sigma_r = 0$ and $\sigma_\theta = 0$), these equations describe a trajectory consisting of alternating arcs, oscillating around a preset direction. In this case, v describes the magnitude of self-propulsion, τ is the period of oscillations in time and the particle turns its velocity vector by the angle $\omega\tau/2$ as it travels along a single arc of its trajectory. When fluctuations are present ($\sigma_r \neq 0$ and $\sigma_\theta \neq 0$), v can be interpreted as the average velocity $\langle|\vec{v}(t)|\rangle$ and $sgn(\sin\,(2\pi t/\tau))\omega$ is the average angular velocity $\langle\dot{\theta}_i(t)\rangle$. The presence of fluctuations introduces random direction changes into the motion of the agents. Depending on the magnitude of fluctuations (given by σ_r and σ_θ) and the specific choice of v and ω, a range of widely different movement patterns can be described by the above model (S1 Figure C,D).

Two extreme examples of simulated movement patterns, spanning the conceptual spectrum of possible behaviors, are ballistic-like motion and free diffusion. Choosing $\sigma_r \ll v$ and $\sigma_\theta \ll \omega$ while keeping non-zero v and ω such that $0 < \omega\tau/2 < \pi$, results in the trajectories resembling the deterministic alternating arcs pattern – or ballistic-like motion. In this case, the agents effectively travel long distances, but do not extensively explore the surroundings of their current position (S1 Figure). In case of $\omega\tau/2 > \pi$ the paths become circular, which can be seen as a quasi-deterministic strategy for more local search. However, the ballistic-like trajectories are generally ‘stiff’, that is, they are characterized by long-persisting correlations in the changes of position. Conversely, assuming $v = 0$ and $\omega = 0$ results in motion akin to passive diffusion. In this case, the agents thoroughly explore their surroundings, but on average do not change position. The correlations in position change are also very short-ranged. The difference between both archetypes of movement pattern is conveniently characterized by the root mean squared displacement:

$$RMSD_i(t) = \sqrt{\langle \left(x_i(t) - x_i(0)\right)^2 \rangle + \langle \left(y_i(t) - y_i(0)\right)^2 \rangle}$$

For ballistic-like motion (with $0 < \omega\tau/2 < \pi$) $RMSD \propto t$, while for free diffusion $RMSD \propto \sqrt{t}$, where in the former case RMSD is the measure of travelled distance, while in the latter case it is a radius of explored area (S1 Figure D). In general, the model (1) can describe a continuity of possible motility patterns (**S1 Figure C**). By varying the parameters of the model (especially, by allowing σ_θ to be comparable with ω, while keeping $v \gg \sigma_r$) it is possible to combine the aspects of ballistic-like motion and free diffusion in almost arbitrary proportions. Significant variety of movement patterns is observed in mammalian sperm, making the proposed movement functions particularly suitable as a model of sperm motility[58,59]; the eventual character of a motility pattern strongly depends on the specific combination of parameter values.

Time in the models advances in discrete steps during which agent states are independently updated in random sequence (i.e. asynchronously). Model-time was scaled to real-time by setting the timestep of an advancement to previously reported beat cross-frequencies for isolated mouse sperm[58]. For example, reported mean beat-cross frequency is 25.4 Hz, and each sperm crosses its average straight-line path once per model-time advancement, then one advancement is approximately 1/25 seconds or 40 milliseconds. The model length and time scales can be readily adjusted to simulate collective behavior of sperm from species other than mouse, but mouse parameters are used throughout this report.

Parameter Estimation for the Sperm Motility Patterns **-** Isolated mouse epididymal sperm have been studied extensively to define the molecular mechanisms and phenotypic characteristics of fertilization competent sperm. Though there is a large set of possible movement characteristics that a given sperm may occupy at a given time, some common features of motility can be classed into specific patterns. For example, ‘progressive’ motility consists of a symmetric movement with low lateral head amplitude about the averaged central path and rapid straight-line movement[56]. Similarly, ‘intermediate’ motility follows a similar movement pattern, but with greater magnitude of lateral head displacement. Here, we define five categorical motility patterns, based on previous work[58].

Typical CASA motility parameters consist of: VAP (average path velocity), VSL (straight line velocity), VCL (curvilinear velocity), ALH (amplitude of lateral head), BCF (beat cross frequency), STR (straightness), and LIN

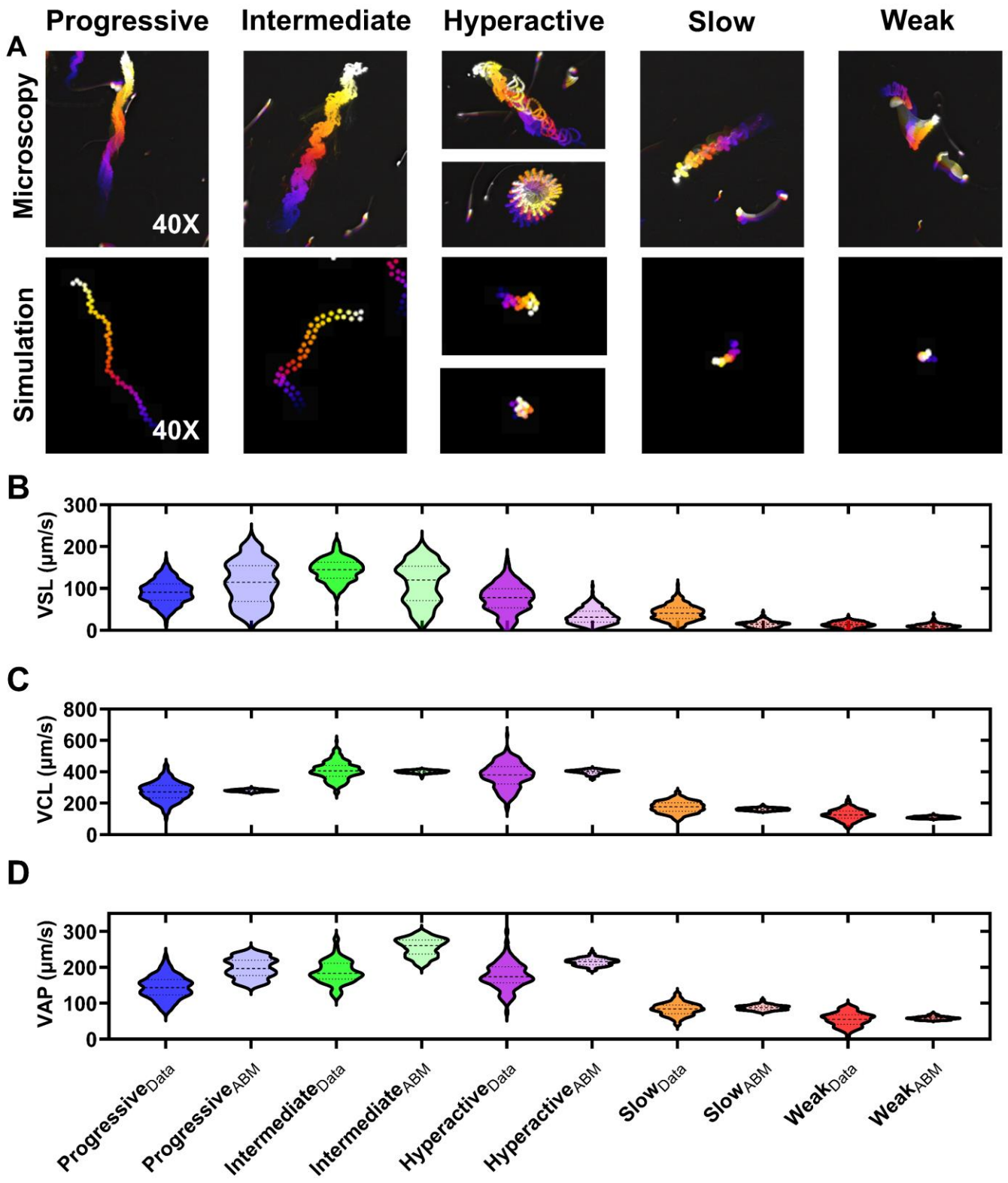

S2 Figure: Converting simple random walkers to artificial sperm. (A) Temporally coded phase contrast images of mouse sperm motility patterns (top row). Matching temporally coded images of simulated sperm-agents for each sperm motility type (bottom row). Color scale is blue (early) to white (late) frames in the video. Simulated trajectories (B) Consensus data from published studies were used to generate normal distributions of curvilinear velocity (VCL) values (indicated by the subscript 'Data'). Parameters (i.e., v(t), θ(t), σ_r, and σ_θ) of each motility type in the agent-based models (i.e., subscript- ABM) were adjusted to approximate the mean VCL values with those identified in the data distributions. N = 250 data points for all groups.

in our models to empirical sperm motility data. Means and standard deviations of the movement parameters for each motility type were obtained from a previous report, and Gaussian distributions were simulated using Graphpad Prism[58]. Temporally-coded phase contrast images of representative cauda epididymal mouse sperm movement patterns at 10X magnification are qualitatively similar to those observed for sperm (shown at approximately 10X magnification at the objective; S2 Figure A). Movement function parameters (VSL, VCL, and VAP) for the agents of each prescribed motility class were adjusted to approximate the distributions sperm movement parameters (S2 Figure 2B-D). The movement function parameter values are detailed in (S1 Table). The distributions did not match exactly for every parameter or motility pattern, indicating that true sperm motility is more complicated than the simple agent rules in this report. Nevertheless, the simulated motility patterns are qualitatively similar to mouse sperm and could be readily updated in future model iterations to accommodate alternative agent rulesets, or movement parameter distributions from other species if labeled CASA data were available. For instances where labeled data is not available, meaning that categorical motility types are not classified, the models could still be fit directly to measured CASA parameter distributions (e.g., VCL, VSL, ALH, etc).

Motility pattern	Nominal Radial Velocity $v[\mu m/s]$	Std. Deviation of Radial Gaussian Noise $\sigma_r[\mu m/s^{1/2}]$	Nominal Angular Velocity $\omega[°/\tau]$	Std. Deviation of Angular Gaussian Noise $\sigma_\theta[°/\tau^{1/2}]$
Progressive	279.4	0.58	45	17.3
Intermediate	419.1	0.29	120	11.5
Hyperactive	419.1	0.29	180	51.0
Slow	152.4	1.15	135	26.0
Weak	101.6	0.29	180	52.0

S1 Table: Movement function parameters for sperm simulations. Parameter to control the oscillation period of the signum function: $\tau = 1/25.4\ [s]$.

Microenvironmental complexity - The microanatomy of mammalian female reproductive tracts imposes spatial limitations on sperm movement that act as physical barriers to eventual contact with the egg(s). In the uterus, the luminal volume is large relative to the size of a single sperm, and convective flow predominates in the dispersion of cells [37]. However, the luminal volume in the cervix and oviducts are much smaller relative to the

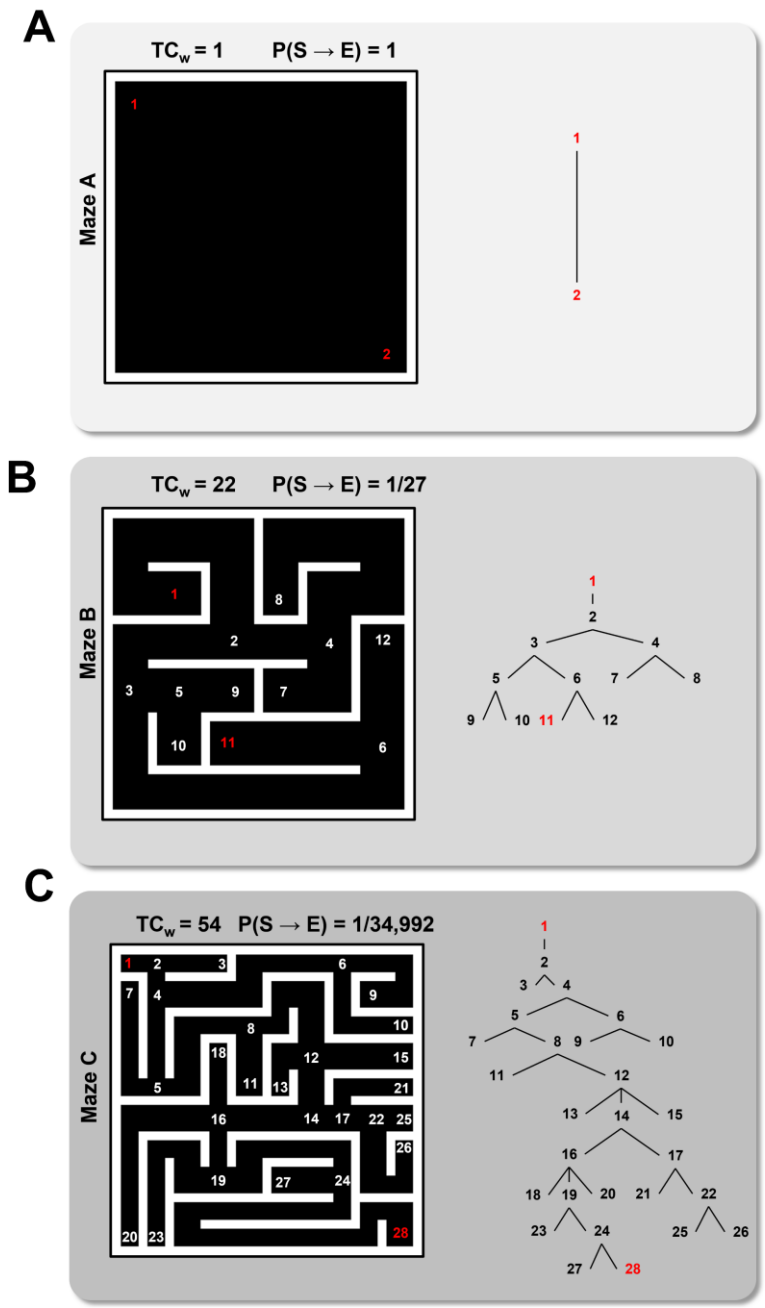

S3 Figure: Modeling Microenvironmental Complexity. (A) The simplest simulation microenvironment consisting of an open space with an egg located in the bottom right corner. Sperm begin at position 1 (red) and end at the egg position 2 (red). TCw = total weighted complexity, a measure of the graph complexity of the maze. P(S→E) = the probability of a sperm taking the shortest direct path to the egg. (B) A more complex maze with increased TCw relative to maze A. (C) The most complex maze used in the simulations. Mazes were constructed using a separate agent-based model in Netlogo. Vertex numbers are indicated on the maze diagrams. Graph networks with numbered vertices connected by edges are shown on the right.

size of a sperm and the relative volumes are constrained by the presence of laminar epithelial folds which form a tight labyrinth-like environment[60].

To model the relationship between microenvironmental complexity and sperm selection, three simulation environments were developed. Mazes (more specifically labyrinths, or 'acyclic' mazes) were chosen as a simple model of microenvironmental spatial complexity because they can be compared quantitatively using foundational concepts from graph theory (S3 Figure). These simple structures are not necessarily intended to serve as accurate models of oviducts, which are much more complex and involve adaptive physiological variables including hormones, metabolites, hydrodynamic forces, and thermal gradients. Rather, the simple mazes enable quantitative exploration of the fundamental constraints imposed on sperm fitness by a selective pressure (in this case- spatial complexity), and can be more readily mimicked *in vitro*, making them more tractable for experimental validation using microfluidics.

The mazes in this report were defined by internal barriers that the sperm could not cross. When a sperm encountered a barrier, the sperm would reorient within a range of possible new directions determined by their motility state and corresponding movement function. The 'egg' was a designated grid square in the environment, and egg-contact occurred when a sperm moved over the square. The mazes consisted of 'dead-ends' and 'intersections' as vertices of an undirected graph $G(v,e)$, where v is a set of vertices $\{v_i\}$ and (e) is a set of edges where e_{ij} *is the unordered vertex pair* $\{v_i, v_j\}$. We define a path as the set of edges that connects two specified vertices. To quantify the complexity of the mazes, the total weighted complexity (TC_w) was calculated as:

$$TC_w = \sum_{i=1}^{k} d_i$$

where d_i is the ith vertex degree (i.e., the total number of paths that lead to and from the vertex) and the vertex indices $\{1, 2, ..., k\}$ is a proper subset of v. An open space in which sperm start at one position and an egg is located at another position within the space, has a total weighted complexity of 1 (S3 Figure A). Mazes with more vertices, or with more edges connecting vertices are more complex and reflect a larger TC_w (S3 Figure B,C). As an additional measure of spatial complexity, we considered the probability of a sperm traversing a direct path from the start (S) position to the (E) egg position, which can be calculated as:

$$P(S \rightarrow E) = \prod_{i=1}^{k} \frac{1}{d_i}$$

where k is the total number of vertices along the shortest path from the sperm to the egg. For example, the probability of a direct path taken (S3 Figure C) is extremely low (i.e., 1/34,992 possible paths).

Time Dependent Changes in Motility Pattern - In this report, sperm are modeled as simple non-adaptive agents. For contrast, an adaptive sperm would be capable of modifying the sensitivity of responses to environmental conditions. Rather, the motility states of the sperm in this report depend only on the pre-defined relationship between the environmental conditions and pre-existing 'perception-action rules' that are stochastically implemented. The behavior of a given sperm is defined by its movement function and sperm in some of the models change movement functions over time via implementation of a time homogeneous Markov process that associates state transitions with a user-defined matrix of probabilities (S2 Table).

Current State	To: Progressive	To: Intermediate	To: Hyperactive	To: Slow	To: Weak
Progressive	0.95	.02	.01	.01	.01
Intermediate	.02	0.94	.02	.01	.01
Hyperactive	.01	.02	0.94	.02	.01
Slow	.00	.01	.02	0.95	.02
Weak	.00	.00	.00	.01	.99

S2 Table: Markov probability transition matrix for changing motility state distributions over time.

Sperm Phenotype Distributions - Mammalian sperm exhibit changes in motility pattern during residence in the female reproductive tract or in chemically-defined media conditions *in vitro* (a maturation process termed- 'capacitation')[61–63]. To incorporate time dependent change in sperm motility phenotypes, spectral flow cytometry was used to assess intracellular calcium distributions among cells under systematically varied incubation conditions. These measurements were then used to aid in updating the agent-based models as described in the following subsections.

Animals - Adult male outbred CD-1 retired breeder mice were obtained from Charles River Laboratories (Raleigh, NC, USA). All work adhered to the guidelines outlined in the National Research Council Guide for the Care and Use of Laboratory Animals and was approved by the Institutional Animal Care and Use Committee of East Carolina University (approval A3469-01). Mice had free access to water and food, were maintained on a 12 hour light/dark cycle and were humanely euthanized by CO2 asphyxiation followed by thoracotomy.

Isolation of mouse epididymal sperm - Testes with epididymides were isolated in phosphate buffered saline (PBS) at 37°C. Cauda epididymides were transferred to isolation media where gently dissected. Following a brief swim-out period (~15 minutes at 37°C), sperm were isolated from epididymal tissue by centrifugation at 100 x g for 2 minutes. Cell counts were determined using a hemocytometer after dilution in water. Cells were then incubated at 37 °C for 30 minutes with 10 µM Indo-1-AM cell permeable free-calcium dye in HEPES buffered, bicarbonate-free, media containing glucose and lactate (2.88 mM and 21 mM respectively). Cells were then washed by centrifugation at 800 x g for 5 minutes.

Calcium clamp and microtiter plate assay - 1 mM EGTA (ethylene glycol-bis(β-aminoethyl ether)-N,N,N′,N′-tetraacetic acid) was used to clamp the 'free' Calcium ion concentration in assay preparations. Calcium concentrations were measured using ion selective electrodes (Kwik Tip electrodes; World Precision Instruments, Sarasota Fl, USA). Two concentration ranges were determined, requiring two separate electrode filling solutions (low range - 150-300 µM; high range - 1.2-2.0 mM) with different concentrations of $CaCl_2$ to obtain an appropriate working range. Once determined, the buffer conditions that clamped the Calcium concentrations were included in the assay in conjunction with sodium bicarbonate pseudo-titrations. pH of the media during the assays did not change and was confirmed using glass tipped pH microelectrodes (World Precision Instruments, Sarasota Fl, USA). Indo-1 stained cells were added into the microtiter plate at unform cell density across the plate and fluorescence (340/400:475 nm) was obtained for ratiometric analysis at 37 °C with sampling every 5 minutes for two hours in a microtiter plate reader (Molecular Devices ID3, San Jose CA, USA). The calcium ionophore ionomycin (10 µM) was used as a positive control.

Spectral Flow cytometry – The qualitative distribution of intracellular calcium in live sperm populations was performed using a 5-laser Aurora spectral analyzer with SpectroFlo acquisition software (V2.2; Cytek, Fremont, CA, USA)[64]. Flow cytometry measurements were performed in capacitating media with corresponding pseudo-titrations of calcium chloride and sodium bicarbonate. Scatter gating was used to identify intact single cells. Live-cell impermeable ToPro3 dye (Thermo Fisher; Waltham MA, USA) was used to monitor cell viability during the assays and mild detergent titrations (digitonin, 24-240 µM) were used to prepare single stain reference for dead cells. Indo-1-AM was excited using a 405nm laser and emission collected at 400 and 475 nm. Conditions were optimized prior to flow cytometry by spectral scanning using a Horiba Duetta fluorometer (Kyoto, Kyoto, Japan). Ionomycin was included as a positive control condition. Scatter plots of fluorescence intensity were manually gated and exported using FlowLogic (V8.7, Inivai Technologies; Victoria AUS). Kernel density estimates of fluorescence ratios for various pseudotitration conditions were plotted using Python (V3.9) with Matplotlib, NumPy, and Pandas libraries.

Data analysis and statistics - Data were analyzed and visualized using Graphpad Prism (V9.1.2), or NumPy, Pandas, and Matplotlib[55,66,67]. Statistical analyses were performed using Graphpad Prism (V9.1.2, San Diego, CA, USA). Two tailed Student's t-test was used for comparison of group means. Normal quantile-quantile

plots were used to assess whether normal based inference procedures should be replaced with nonparametric methods. The presence of outliers, both their magnitude and number, was also used to check the assumptions of inference procedures. For multifactorial designs one- or two-way ANOVA was performed for one or two factor designs, with Dunnett or Sidak *post hoc* tests for multiple comparison respectively. All data are presented as raw values with the median represented by a bar. An α value of 0.05 was used as the threshold of statistical significance.

Conclusion

In this report we developed agent-based models (ABMs) and explored aspects of collective behavior of non-adaptive sperm (i.e. sperm that change motility pattern over time in a manner that depends on intrinsic control, rather than exogenous responses to signals). Our results highlight the intertwined influences of microenvironmental complexity and sperm phenotypic heterogeneity in shaping sperm fitness- defined here as the probability of egg contact given that a sperm has a particular trait value. Results from this study provide key insights and useful definitions for the further exploration of a theory of sperm selection in the context of ART. The insights provided by the models hold promise for optimizing real-time sperm diagnostics and selection strategies with broad applications in both clinical and agricultural settings.

Author Contributions

BB, KC, SS, LH, AC, CD, IH, EC, MM, HB, DH, and CAS designed, built, and tested the agent-based models. BB, AC, IH, MM, DB, and CAS designed and implemented data collection for the multi-dimensional culture arrays and spectral flow cytometry. KC and CAS designed, tested, and implemented Python programs for analysis of ABM data. PV and CAS performed statistical design analysis. MB, MM, and CAS developed and validated sperm movement functions for the ABMs. All co-authors reviewed and edited the work. BB, KC, MM, and CAS authored manuscript drafts and performed final editing.

Funding

This work was supported by the Eunice Kennedy Shriver National Institute of Child Health and Human Development (R01HD110170), as well as laboratory startup funding from the Thomas Harriot College of Arts and Sciences at East Carolina University and the East Carolina University Research and Economic Development Office. The funders had no role in study design, data collection and analysis, decision to publish, or preparation of the manuscript.

Disclosures

The authors declare no conflicts of interest.

Acknowledgements

None

Cited References

1. Kandel ME, Rubessa M, He YR, Schreiber S, Meyers S, Matter Naves L, et al. Reproductive outcomes predicted by phase imaging with computational specificity of spermatozoon ultrastructure. 2020;2020: 18302–18309. doi:10.1073/pnas.2001754117/-/DCSupplemental

2. You JB, McCallum C, Wang Y, Riordon J, Nosrati R, Sinton D. Machine learning for sperm selection. Nature Reviews Urology. Nature Research; 2021. pp. 387–403. doi:10.1038/s41585-021-00465-1

3. Oehninger S, Franken DR, Ombelet W. Sperm functional tests. Fertility and Sterility. Elsevier Inc.; 2014. pp. 1528–1533. doi:10.1016/j.fertnstert.2014.09.044

4. Buffone MG, Doncel GF, Briggiler CIM, Vazquez-Levin MH, Calamera JC. Human sperm subpopulations: Relationship between functional quality and protein tyrosine phosphorylation. Human Reproduction. 2004;19: 139–146. doi:10.1093/humrep/deh040

5. Molina LCP, Luque GM, Balestrini PA, Marín-Briggiler CI, Romarowski A, Buffone MG. Molecular basis of human sperm capacitation. Frontiers in Cell and Developmental Biology. Frontiers Media S.A.; 2018. doi:10.3389/fcell.2018.00072

6. Luque GM, Dalotto-Moreno T, Martín-Hidalgo D, Ritagliati C, Puga Molina LC, Romarowski A, et al. Only a subpopulation of mouse sperm displays a rapid increase in intracellular calcium during capacitation. J Cell Physiol. 2018;233: 9685–9700. doi:10.1002/jcp.26883

7. Navarrete FA, Aguila L, Martin-Hidalgo D, Tourzani DA, Luque GM, Ardestani G, et al. Transient Sperm Starvation Improves the Outcome of Assisted Reproductive Technologies. Front Cell Dev Biol. 2019;7: 1–13. doi:10.3389/fcell.2019.00262

8. Darszon A, Nishigaki T, López-González I, Visconti PE, Treviño CL. Differences and similarities: The richness of comparative sperm physiology. Physiology. 2020;35: 196–208. doi:10.1152/physiol.00033.2019

9. Aguado-García A, Priego-Espinosa DA, Aldana A, Darszon A, Martínez-Mekler G. Mathematical model reveals that heterogeneity in the number of ion transporters regulates the fraction of mouse sperm capacitation. PLoS One. 2021;16. doi:10.1371/journal.pone.0245816

10. Schmidt CA, Hale BJ, Bhowmick D, Miller WJ, Neufer PD, Geyer CB. Pyruvate modulation of redox potential controls mouse sperm motility. Dev Cell. 2023. doi:10.1016/j.devcel.2023.11.011

11. Parker GA. SPERM COMPETITION AND ITS EVOLUTIONARY CONSEQUENCES IN THE INSECTS. Biol Rev. 1970;45: 525–567.

12. Tourmente M, Gomendio M, Roldan ERS. Sperm competition and the evolution of sperm design in mammals. BMC Evol Biol. 2011;11. doi:10.1186/1471-2148-11-12

13. Simmons LW, Fitzpatrick JL. Sperm wars and the evolution of male fertility. Reproduction. 2012. pp. 519–534. doi:10.1530/REP-12-0285

14. Sutter A, Immler S. Within-ejaculate sperm competition. Philosophical Transactions of the Royal Society B: Biological Sciences. Royal Society Publishing; 2020. doi:10.1098/rstb.2020.0066

15. Firman RC, Gasparini C, Manier MK, Pizzari T. Postmating Female Control: 20 Years of Cryptic Female Choice. Trends in Ecology and Evolution. Elsevier Ltd; 2017. pp. 368–382. doi:10.1016/j.tree.2017.02.010

16. Suarez SS. Control of hyperactivation in sperm. Human Reproduction Update. 2008. pp. 647–657. doi:10.1093/humupd/dmn029

17. Aleliunas R, Arp RMK, Lipton RJ, Lovasz L, Rackoff C. Random Walks, Universal Traversal Sequences, and the Complexity of Maze Problems. Annual Symposium on Foundations of Computer Science. 1979.

18. Travis AJ, Jorgez CJ, Merdiushev T, Jones BH, Dess DM, Diaz-Cueto L, et al. Functional Relationships between Capacitation-dependent Cell Signaling and Compartmentalized Metabolic Pathways in Murine Spermatozoa. Journal of Biological Chemistry. 2001;276: 7630–7636. doi:10.1074/jbc.M006217200

19. Balbach M, Gervasi MG, Hidalgo DM, Visconti PE, Levin LR, Buck J. Metabolic changes in mouse sperm during capacitation†. Biol Reprod. 2020. doi:10.1093/biolre/ioaa114

20. Visconti PE, Moore GD, Bailey JL, Leclerc P, Connors SA, Pan D, et al. Capacitation of mouse spermatozoa. II. Protein tyrosine phosphorylation and capacitation are regulated by a cAMP-dependent pathway. Development. 1995;121: 1139–1150. doi:10.1242/DEV.121.4.1139

21. Hereng TH, Elgstøen KBP, Cederkvist FH, Eide L, Jahnsen T, Sklhegg BS, et al. Exogenous pyruvate accelerates glycolysis and promotes capacitation in human spermatozoa. Human Reproduction. 2011;26: 3249–3263. doi:10.1093/humrep/der317

22. Orta G, De La Vega-Beltran JL, Martín-Hidalgo XD, Santi CM, Visconti PE, Darszon XA. CatSper channels are regulated by protein kinase A. Journal of Biological Chemistry. 2019;293: 16830–16841. doi:10.1074/jbc.RA117.001566

23. Codling EA, Plank MJ, Benhamou S. Random walk models in biology. Journal of the Royal Society Interface. Royal Society; 2008. pp. 813–834. doi:10.1098/rsif.2008.0014

24. Larralde H. First-passage probabilities and mean number of sites visited by a persistent random walker in one- And two-dimensional lattices. Phys Rev E. 2020;102. doi:10.1103/PhysRevE.102.062129

25. Larralde H, Trunfio P, Havlin S, Stanley HE, Weiss GH. Number of distinct sites visited by N random walkers. Phys Rev A (Coll Park). 1992;45.

26. Baker MA, Reeves G, Hetherington L, Aitken RJ. Analysis of proteomic changes associated with sperm capacitation through the combined use of IPG-strip prefractionation followed by RP chromatography LC-MS/ MS analysis. Proteomics. 2010;10: 482–495. doi:10.1002/pmic.200900574

27. Ferramosca A, Zara V. Bioenergetics of mammalian sperm capacitation. Biomed Res Int. 2014;2014. doi:10.1155/2014/902953

28. Inoue N, Hamada D, Kamikubo H, Hirata K, Kataoka M, Yamamoto M, et al. Molecular dissection of IZUMO1, a sperm protein essential for sperm-egg fusion. Development (Cambridge). 2013;140: 3221–3229. doi:10.1242/dev.094854

29. Naokazu Inoue, Masahito Ikawa, Ayako Isotani, Masaru Okabe. The immunoglobulin superfamily protein Izumo is required for sperm to fuse with eggs. Nature. 2005;434: 229–234. doi:10.1038/nature03318

30. Cardullo RA, Baltz JM. Metabolic regulation in mammalian sperm: Mitochondrial volume determines sperm length and flagellar beat frequency. Cell Motil Cytoskeleton. 1991;19: 180–188. doi:10.1002/cm.970190306

31. Gallagher MT, Cupples G, Ooi EH, Kirkman-Brown JC, Smith DJ. Rapid sperm capture: High-throughput flagellar waveform analysis. Human Reproduction. 2019;34: 1173–1185. doi:10.1093/humrep/dez056

32. Lighthill JT. Flagellar Hydrodynamics. SIAM Review. 1976;18: 161–226. Available: https://about.jstor.org/terms

33. Miller MR, Kenny SJ, Mannowetz N, Mansell SA, Wojcik M, Mendoza S, et al. Asymmetrically Positioned Flagellar Control Units Regulate Human Sperm Rotation. Cell Rep. 2018;24: 2606–2613. doi:10.1016/j.celrep.2018.08.016

34. Ooi EH, Smith DJ, Gadêlha H, Gaffney EA, Kirkman-Brown J. The mechanics of hyperactivation in adhered human sperm. R Soc Open Sci. 2014;1. doi:10.1098/rsos.140230

35. Martínez-Pastor F. What is the importance of sperm subpopulations? Anim Reprod Sci. 2022;246. doi:10.1016/j.anireprosci.2021.106844

36. Yang J, Kupka I, Schuss Z, Holcman D. Search for a small egg by spermatozoa in restricted geometries. J Math Biol. 2016;73: 423–446. doi:10.1007/s00285-015-0955-3

37. Suarez SS, Pacey AA. Sperm transport in the female reproductive tract. Hum Reprod Update. 2006;12: 23–37. doi:10.1093/humupd/dmi047

38. Baldini D, Ferri D, Baldini GM, Lot D, Catino A, Vizziello D, et al. Sperm selection for icsi: Do we have a winner? Cells. MDPI; 2021. doi:10.3390/cells10123566

39. Nosrati R, Graham PJ, Zhang B, Riordon J, Lagunov A, Hannam TG, et al. Microfluidics for sperm analysis and selection. Nature Reviews Urology. Nature Publishing Group; 2017. pp. 707–730. doi:10.1038/nrurol.2017.175

40. Cohen J. Cross-Overs, Sperm Redundancy and Their Close Association. Heredity (Edinb). 1973;31: 408–413.

41. Roldan ERS. Sperm competition and the evolution of sperm form and function in mammals. Reproduction in Domestic Animals. 2019;54: 14–21. doi:10.1111/rda.13552

42. Villani MT, Morini D, Spaggiari G, Falbo AI, Melli B, La Sala GB, et al. Are sperm parameters able to predict the success of assisted reproductive technology? A retrospective analysis of over 22,000 assisted reproductive technology cycles. Andrology. 2022;10: 310–321. doi:10.1111/andr.13123

43. Donnelly ET, Lewis SEM, Mcnally JA, Thompson W. In vitro fertilization and pregnancy rates: the influence of sperm motility and morphology on IVF outcome. Fertil Steril. 1998;70: 305–314.

44. Shalom-Paz E, Anabusi S, Michaeli M, Karchovsky-Shoshan E, Rothfarb N, Shavit T, et al. Can intra cytoplasmatic morphologically selected sperm injection (IMSI) technique improve outcome in patients with repeated IVF–ICSI failure? a comparative study. Gynecological Endocrinology. 2015;31: 247–251. doi:10.3109/09513590.2014.982085

45. Frank SA. Natural selection. V. How to read the fundamental equations of evolutionary change in terms of information theory. Journal of Evolutionary Biology. 2012. pp. 2377–2396. doi:10.1111/jeb.12010

46. Gómez Montoto L, Magaña C, Tourmente M, Martín-Coello J, Crespo C, Luque-Larena JJ, et al. Sperm competition, sperm numbers and sperm quality in muroid rodents. PLoS One. 2011;6. doi:10.1371/journal.pone.0018173

47. Petrunkina AM, Waberski D, Günzel-Apel AR, Töpfer-Petersen E. Determinants of sperm quality and fertility in domestic species. Reproduction. 2007. pp. 3–17. doi:10.1530/REP-07-0046

48. Fernández-López P, Garriga J, Casas I, Yeste M, Bartumeus F. Predicting fertility from sperm motility landscapes. Commun Biol. 2022;5. doi:10.1038/s42003-022-03954-0

49. Riordon J, McCallum C, Sinton D. Deep learning for the classification of human sperm. Comput Biol Med. 2019;111. doi:10.1016/j.compbiomed.2019.103342

50. Baez JC, Pollard BS. Relative entropy in biological systems. Entropy. MDPI AG; 2016. doi:10.3390/e18020046

51. Frank SA. Natural selection maximizes Fisher information. Journal of Evolutionary Biology. 2009. pp. 231–244. doi:10.1111/j.1420-9101.2008.01647.x

52. Kromer JA, Märcker S, Lange S, Baier C, Friedrich BM. Decision making improves sperm chemotaxis in the presence of noise. PLoS Comput Biol. 2018;14. doi:10.1371/journal.pcbi.1006109

53. de Prelle B, Lybaert P, Gall D. A Minimal Model Shows that a Positive Feedback Loop Between sNHE and SLO3 can Control Mouse Sperm Capacitation. Front Cell Dev Biol. 2022;10. doi:10.3389/fcell.2022.835594

54. Tisue S, Wilensky U. NetLogo: A Simple Environment for Modeling Complexity. International conference on complex systems. Boston, MA; 2004. pp. 16–21.

55. Harris CR, Millman KJ, van der Walt SJ, Gommers R, Virtanen P, Cournapeau D, et al. Array programming with NumPy. Nature. Nature Research; 2020. pp. 357–362. doi:10.1038/s41586-020-2649-2

56. Hansen JN, Jikeli J, Wachten D. SpermQ–a simple analysis software to comprehensively study flagellar beating and sperm steering. Cells. 2018;1. doi:10.1101/449173

57. Gallagher MT, Cupples G, Ooi EH, Kirkman-Brown JC, Smith DJ. Rapid sperm capture: High-throughput flagellar waveform analysis. Human Reproduction. 2019;34: 1173–1185. doi:10.1093/humrep/dez056

58. Goodson SG, Zhang Z, Tsuruta JK, Wang W, O'Brien DA. Classification of mouse sperm motility patterns using an automated multiclass support vector machines model. Biol Reprod. 2011;84. doi:10.1095/biolreprod.110.088989

59. Goodson SG, White S, Stevans AM, Bhat S, Kao C-Y, Jaworski S, et al. CASAnova: a multiclass support vector machine model for the classification of human sperm motility patterns†. Biol Reprod. 2017;97: 698–708. doi:10.1093/biolre/iox120

60. Giojalas LC, Guidobaldi HA. Getting to and away from the egg, an interplay between several sperm transport mechanisms and a complex oviduct physiology. Molecular and Cellular Endocrinology. Elsevier Ireland Ltd; 2020. p. 110954. doi:10.1016/j.mce.2020.110954

61. Gervasi MG, Visconti PE. Chang's meaning of capacitation: A molecular perspective. Molecular Reproduction and Development. John Wiley and Sons Inc.; 2016. pp. 860–874. doi:10.1002/mrd.22663

62. Suarez SS. Control of hyperactivation in sperm. Human Reproduction Update. Oxford Academic; 2008. pp. 647–657. doi:10.1093/humupd/dmn029

63. Chang H, Suarez SS. Rethinking the relationship between hyperactivation and chemotaxis in mammalian sperm. Biology of Reproduction. Oxford Academic; 2010. pp. 507–513. doi:10.1095/biolreprod.109.083113

64. Park LM, Lannigan J, Jaimes MC. OMIP-069: Forty-Color Full Spectrum Flow Cytometry Panel for Deep Immunophenotyping of Major Cell Subsets in Human Peripheral Blood. Cytometry Part A. 2020;97: 1044–1051. doi:10.1002/cyto.a.24213

65. Miller MR, Kenny SJ, Mannowetz N, Mansell SA, Wojcik M, Mendoza S, et al. Asymmetrically Positioned Flagellar Control Units Regulate Human Sperm Rotation. Cell Rep. 2019;26. doi:10.1016/j.celrep.2019.02.075

66. Hunter JD. Matplotlib: A 2D graphics environment. Computing in science & engineering. 2007. pp. 90–95.

67. Mckinney W. Data Structures for Statistical Computing in Python. SciPy . 2010;445.